Available online at www.sciencedirect.com
SCIENCE DIRECT®

Journal of the European Ceramic Society 24 (2004) 2769–2783
www.elsevier.com/locate/jeurceramsoc

Mechanical and microstructural characterisation of Nextel 650 alumina–zirconia fibres

A. Poulon-Quintin, M.H. Berger, A.R. Bunsell*

Ecole des Mines de Paris, Centre des Matériaux, BP 87, Evry Cedex, France

Received 28 April 2003; received in revised form 18 August 2003; accepted 21 August 2003

Abstract

A two-phase alumina–zirconia fibre, the Nextel 650 fibre (3M), has been studied in tension and creep up to 1300 °C. Microstructural investigations on as-received and tested fibres have been conducted in parallel. Compared to current commercially available fine oxide fibres (alumina and alumina–zirconia based), the fibre shows good creep resistance despite a smaller alumina grain size. High temperature deformation of the fibre is achieved by grain-boundary sliding and is accompanied by oriented alumina grain growth. Sensitivity to alkaline contamination is shown by fast α-alumina grain growth at the fibre surface.

Keywords: Al_2O_3; Creep; Fibres; Microstructure; Nextel 650; ZrO_2

1. Introduction

Oxide fibres have an obvious chemical advantage over non-oxide fibres for use at high temperatures in oxidizing or corrosive environments. Many polycrystalline oxide fibres have been developed for both refractory insulation and structural reinforcements. These fibres are mainly based on alumina but they have been found to suffer from loss of strength and creep from around 1000 °C. However, creep behaviour of polycrystalline alumina can be improved by the inclusion of zirconia particles which act to pin the structure and modify intergranular diffusion. This was clearly shown by the comparison of the creep behaviours of the PRD-166 fibre containing 20 wt.% of yttria stabilised tetragonal zirconia and the pure alumina Fibre FP, both produced by Du Pont.[1] These fibres had diameters of about 20 μm and as a consequence, combined with their high Young's moduli, both showed poor flexibility, which made weaving impossible.

The flexibility of a fibre is related to the reciprocal of the cube of its diameter. As a result, more recent fibres have smaller diameters. Minnesota Mining and Manufacturing (3M) produces sol-based fibres such as the Nextel 610 (α-alumina fibre), the Nextel 650 fibre (zirconia reinforced α-alumina fibre) and the Nextel 720 (alumina-mullite fibre). All of them have small diameters (respectively 11, 11 and 12.5 μm). Moreover, smaller grain sizes have been obtained compared to those of the DuPont's fibres of similar compositions, by the addition of iron compounds as nucleating agents and SiO_2. The Nextel 720 fibre showed the highest creep resistance up to 1500 °C of all current commercial fine oxide fibres but also a high sensitivity to alkaline contamination.[2] The Nextel 610, a pure alumina fibre produced by 3M, showed comparable creep properties to the Fibre FP (up to 1200 °C) but compared to those of the PRD-166 and the Nextel 720, they were poor.[3] As a result the Nextel 650 fibre was created by 3M, in order to combine the properties of a fibre which firstly was resistant to alkalines, as this was important for a reinforcement for high temperature composites, and secondly had improved creep resistance compared to the Nextel 610 fibre.

The aim of this paper is to determine the high temperature behaviour of the Nextel 650 α-alumina/zirconia fibre. The role of the fibre microstructure and the effect of the additives on its mechanical behaviour have been investigated in parallel with a study of the evolution, under load at high temperature, of its mechanical properties and microstructure.

* Corresponding author. Tel.: +33-1-60-76-3015; fax: +33-1-60-76-3150.
E-mail address: anthony.bunsell@ensmp.fr (A.R. Bunsell).

0955-2219/$ - see front matter © 2003 Elsevier Ltd. All rights reserved.
doi:10.1016/j.jeurceramsoc.2003.08.011

2. Experimental procedure

Great care was taken not to contaminate the fibres during handling and tweezers were always used so as to avoid contact with the skin.

All the observations of the failure surfaces and of the external surfaces of the fibres after tensile or creep tests were made using a LEO DSM982 Gemini Field Emission Gun Scanning Electron Microscope at acceleration voltages between 1 and 5 kV.

The microstructures of the fibres were investigated using a PHILIPS EM430 Transmission Electron Microscope with an acceleration voltage of 300 kV. Thin foils were obtained by ion milling, using methods described elsewhere.[4]

A Siemens D500 X-ray diffractometer was used to analyse the crystallographic orientation of the alumina and zirconia grains before and after their evolution during high temperature loading. For each fibre bundle, two spectra were obtained in transmission. The position of the fibre bundle in the plane perpendicular to beam was either horizontal $\varphi = 0$ or vertical $\varphi = 90$ (see Fig. 1).

Single filaments were tested in tension up to 1300 °C and in creep up to 1250 °C, on a horizontal tensile machine with a cross-head speed of 0.04 mm/s and force sensitivity of 10^{-2} N [5]. The diameters of the fibres were measured prior to each test on single fibres using a Mitutoyo Laser Scan Micrometer LSM-6000 giving an accuracy of 0.1 μm.

Bundles of fibres were tested in creep up to 1300 °C on a horizontal tensile machine with a cross-head speed of 0.04mm/s and a force sensitivity of 0.5 N [5]. As the Young's modulus of the fibre and the compliance of the tensile machine were known, a simple calculation, from the initial slope obtained in tension at room temperature, allowed the number of fibres loaded in a bundle to be estimated with an accuracy better than 90%.

The use of resistance ovens composed of a Kanthal super heating element (for single fibres) or a lanthanum chromite heating element (for bundles) placed around an alumina inner tube allowed the fibres to be tested at high temperature with extremely rapid heat-up rates. The grips remained cold and the length of the hottest part of the furnace was 25 mm for the single fibre tests and 40 mm for tests on bundles. The test temperature was maintained within the hot part of the furnace to within ±25 °C for both single filaments and bundles.

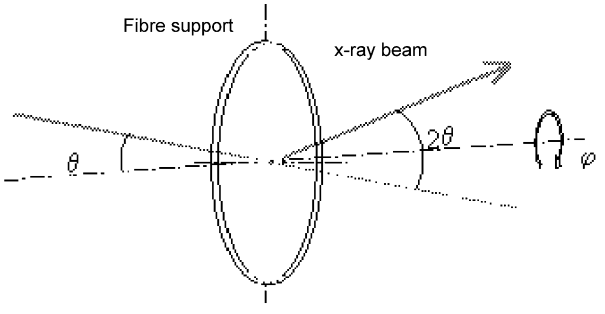

Fig. 1. Diagram of the X-ray spectrum acquisition.

3. As-received fibre and thermal stability

The Nextel 650 fibre is a continuous circular fibre produced by a sol-gel manufacturing route. The fibre has a diameter of 11.2μm and is composed of α-alumina with 10 wt.% of cubic zirconia stabilized by 1 wt.% of Y_2O_3. Zirconia has been added to increase the elongation to failure and to limit alumina grain growth. Chemical analysis indicated that the fibre contained 0.4 wt.% Fe used as a nucleating agent for the formation of α-alumina, a few ppm of Na, K, Ca and Cl ($<<0.1$ wt.%) in the bulk of the fibre and a significant quantity of Si (0.15 wt.%). Moreover, on the fibre surface, WDX analysis showed the presence of impurity-rich clusters (size <1 μm).

The microstructure obtained is presented in Fig. 2. The alumina grain size was 0.1 μm. The zirconia grain size was seen to be bimodal consisting of intra-granular grains of 5–10 nm in size and inter-granular grains of 20–30 nm as shown in Fig. 2b. No other second phase was detected by high resolution TEM of the as-received fibre. Intergranular porosity was almost non-existent. High resolution TEM also showed that the α-alumina grains were twinned and not facetted. This phenomenon is typical of fine grain alumina obtained by rapid pyrolysis.

Even though there was no anisotropy in the grain shape, the X-ray study showed the existence of an overall crystallographic anisotropy. Fig. 3 shows diffractograms obtained for a horizontal and vertical orientations with respect to the beam for the same bundle. The ratios of peak areas corresponding to the almost perpendicular planes {1 0 . 10} and {0 3 . 0} were studied. The peak corresponding to the plane {0 0 . 1} could not be used for this analysis because of its low intensity. The ratio value A{1 0 . 10}/ A{0 3 . 0} was higher than 1 for $\varphi = 0$ but significantly lower than 1 for $\varphi = 90$. These results showed that the basal plane was preferentially aligned with the fibre axis.

After heat treatment in air, the preferential crystallographic orientation with respect to the fibre axis was confirmed when the fibres were heat treated under load (1250 °C, 20 MPa, 34 h) or without load (1400 °C, 6 h or 24 h). The evolution of the ratios between the areas of chosen peaks were studied. After heat treatment at 1400 °C for 24 h, this ratio was increased from 2 for as-received fibres to 8, as can be seen from Fig. 4. These results confirmed conclusions based on the observations of the alumina grain shape. After a heat treatment of 24 h without load at 1400 °C, the sizes of alumina grains were increased up to 100 times their initial size, as shown in Fig. 5, and were aligned approximately with

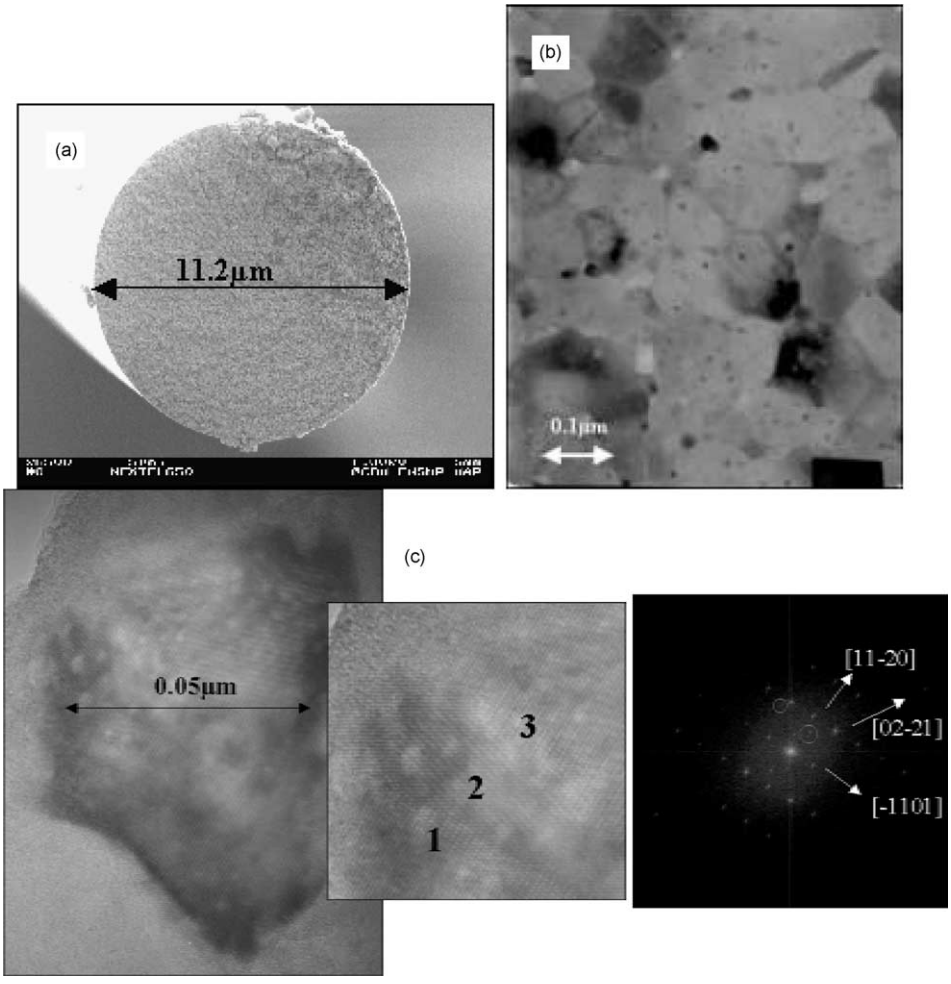

Fig. 2. The Nextel 650 fibre: (a) fracture surface at room temperature, fibre (b) and alumina grain (c) microstructures (TEM picture).

the fibre axis. An increase of the zirconia inter-granular grain size was observed mostly due to re-organisation of the grains at the grain boundaries. Moreover, abnormal alumina grain growth was noticed locally (chemical analyses of the corresponding zone showed the presence of Si, Na, Ca and K) together with an increase of the fiber diameter and the creation of very porous areas, both of which weakened the fibre. After heat treatment under load (1250 °C, 20 MPa, 34 h), the alignment of the alumina grains with the load axis (i.e. the fibre axis) became more obvious, as is revealed by Fig. 6. The mean alumina grain size was 1.1 ± 0.6 µm and the intergranular zirconia grain size was 0.10 ± 0.05 µm. No change in the intragranular zirconia grain size was noticed. A study of the planar interfaces of the alumina grains aligned with the fibre axis showed that these planes corresponded to the basal plane and that there was an amorphous phase at the grain boundaries in which, EDX analysis revealed the presence of a significant silicon peak, as shown in Fig. 6.

4. Mechanical behaviour

4.1. Tensile strength

4.1.1. At high temperature

The tensile strengths of single fibres were measured from room temperature up to 1300 °C. For most temperatures at least twenty five fibres were tested in order to obtain the median strength. Above 1100 °C, plastic deformation was observed on the load-displacement curves. The fibre median strength remained almost constant up to 700 °C and was equal to 2.3 ± 0.3 GPa. The Young's modulus was estimated to be equal to 370 GPa.

At 800 °C, only 73% of the room temperature failure strength was retained (a phenomenon also observed at 800 °C for the Nextel 610 which retained 70% of initial failure strength), 30% at 1200 °C and only 6% at 1300 °C, as shown in Fig. 7. Failure strains at 1300 °C could reach 10 times those at room temperature.

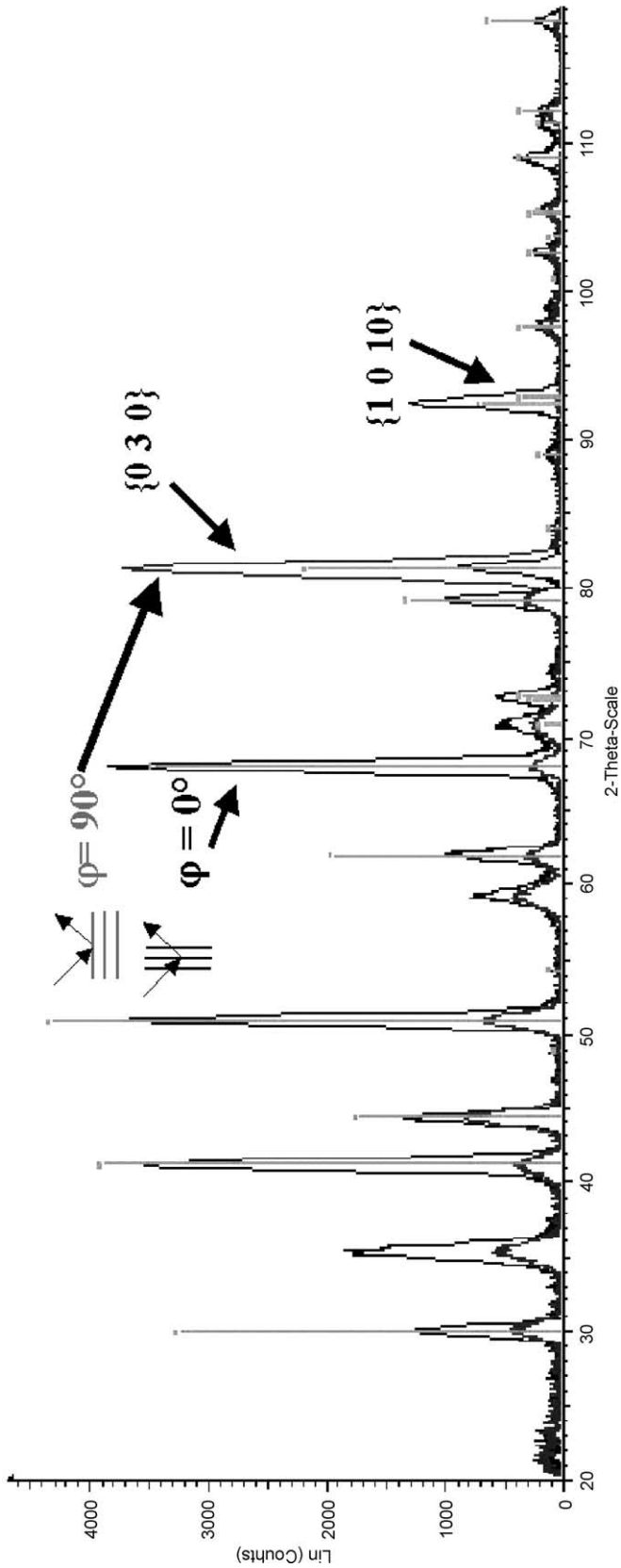

Fig. 3. X-ray spectrums of the as-received fibre: $\varphi = 0$ (dark) and $\varphi = 90°$ (grey).

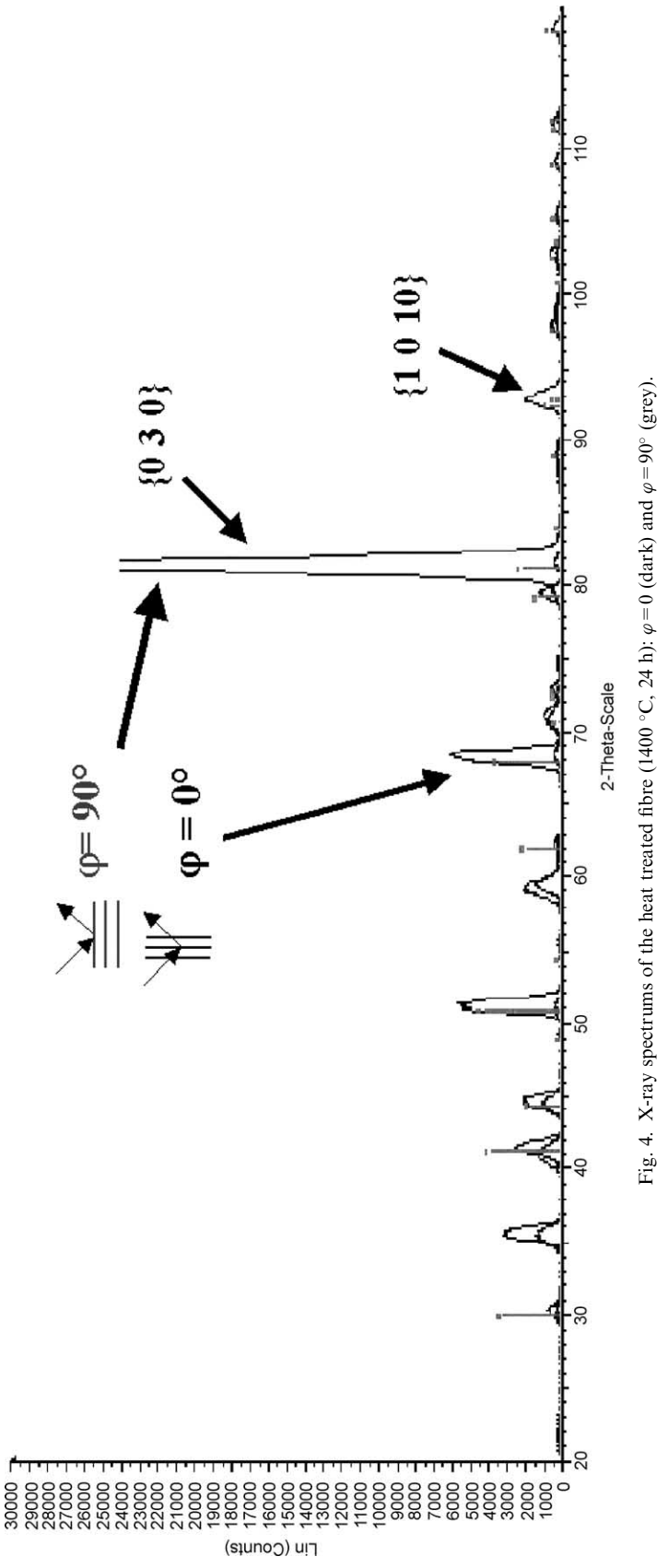

Fig. 4. X-ray spectrums of the heat treated fibre (1400 °C, 24 h): $\varphi = 0$ (dark) and $\varphi = 90°$ (grey).

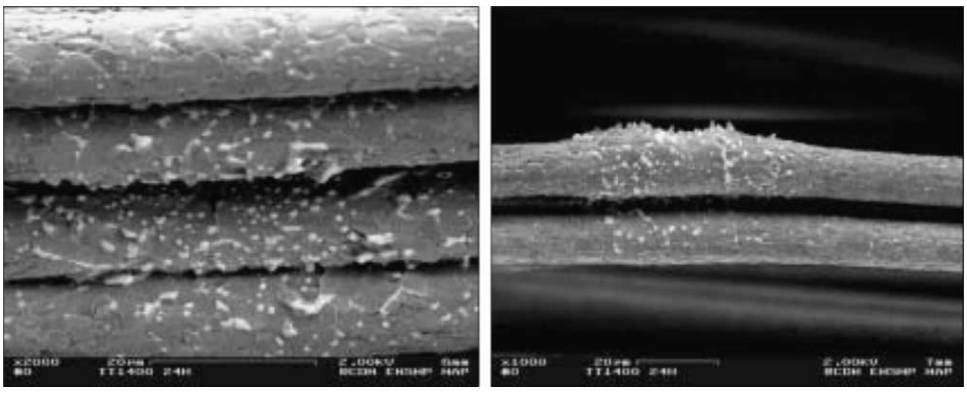

Fig. 5. The Nextel 650 fibres after heat treatment in air at 1400 °C for 24 h.

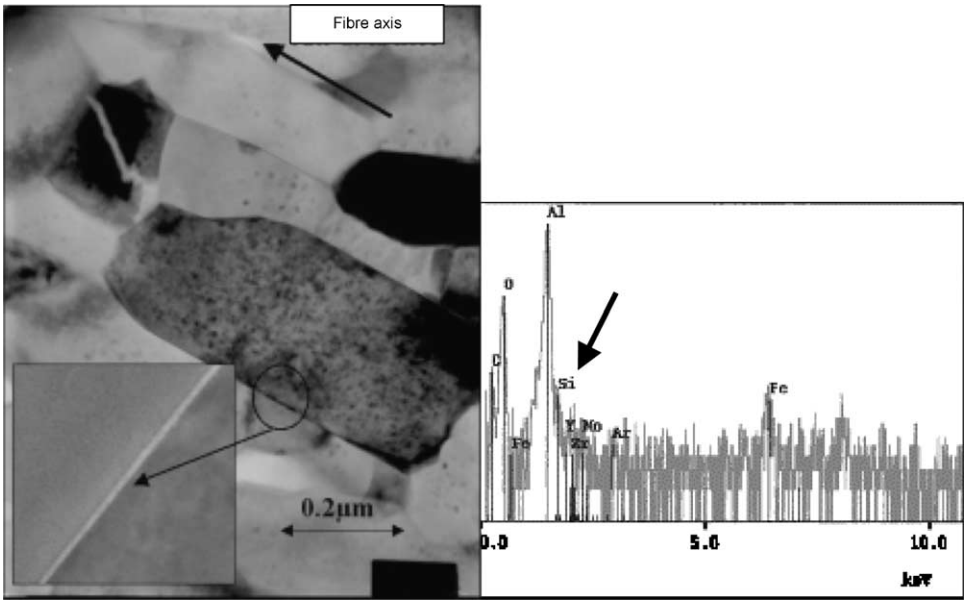

Fig. 6. Presence of an amorphous phase at the grain boundaries of the linear face of the alumina fibre axis aligned grains obtained after heat treatment under load (1250 °C, 20 MPa, 34 h): TEM picture and EDX spectrum revealing the presence of Si at this grain boundary.

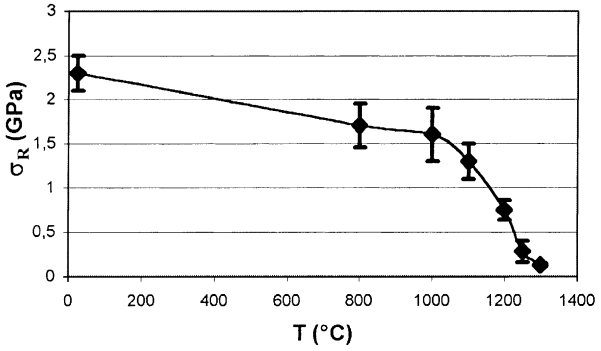

Fig. 7. Strength evolution as a function of the temperature.

4.1.2. Fracture morphology

Single fibre fracture surfaces exhibited a similar appearance to that at room temperature up to 1100 °C, showing a plane surface and mostly intergranular crack propagation. Even if there was no general grain growth, some failure surfaces presented an area at the periphery of the fibre with abnormal alumina grain growth at all temperatures (see Fig. 8). EDX analysis revealed a high concentration of the elements Si and Ca.

At and above 1200 °C, the mode of rupture remained inter-granular. Failure surfaces were still planar but showed increasingly abnormal alumina grain growth. The higher the temperature was, the more the presence of impurities on the fibre surface was critical in leading to spectacular platelet alumina grain growth as shown in Fig. 8.

At 1200 °C, the failure surfaces, showed two different areas and became more prominent at 1250 °C, as can be seen in Fig. 9. The first was a "rough" non planar area corresponding to slow crack propagation at high temperature and the second by opposition was planar, corresponding to rapid crack propagation. Moreover, isotropic grain growth of the grains (0.2 µm) was observed at the fibre surface. The failure mechanism corresponding to the rough area was identified as sub-critical

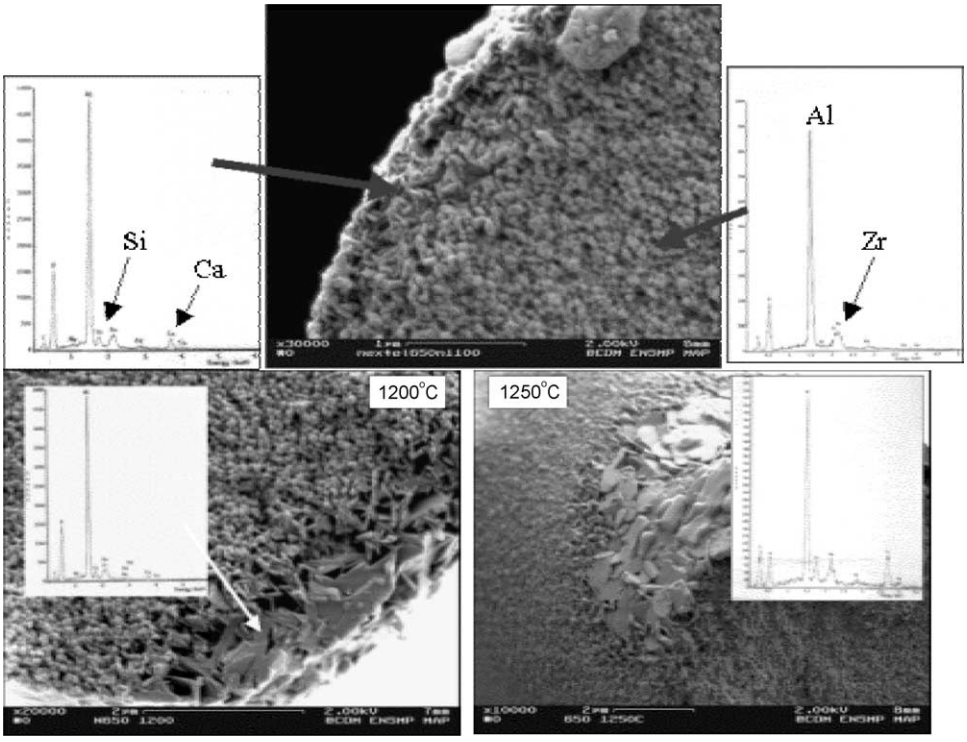

Fig. 8. Particularities observed on failure surfaces at 1100, 1200 and 1250 °C. EDX analysis results.

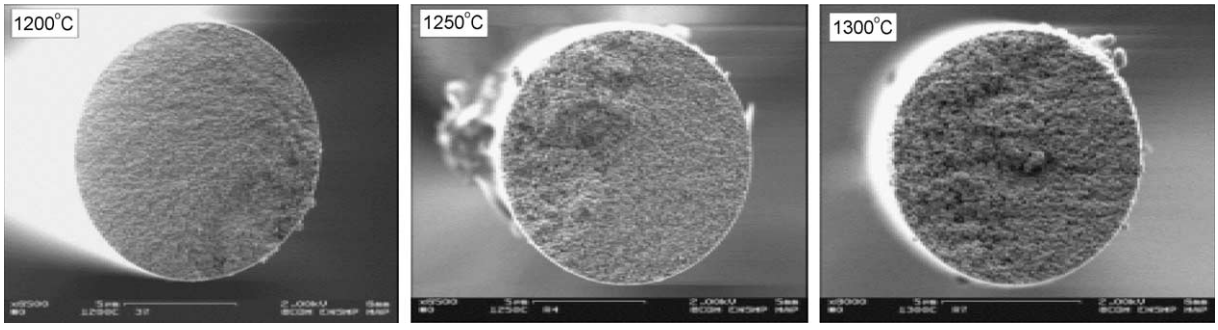

Fig. 9. Failure surfaces at high temperatures (from 1200 to 1300 °C).

crack growth, which is a mechanism very sensitive to the glassy phase present at grain boundaries. The rough surface area increased as the temperature increased, as can be seen to have occurred at 1300 °C. When alumina grain growth occurred under load, slow crack propagation started from the surface defect areas and then was followed by rapid failure. Moreover, grain growth was noticed in the slow crack area.

4.2. Creep behaviour

4.2.1. Creep test results

Bundles of fibres and single filaments were tested in creep up to 1300 and 1250 °C respectively. No significant creep occurred below 1100 °C. For all temperatures, very little primary creep was observed. Steady state creep could be followed by tertiary creep, depending on the applied load and the temperature. Tertiary creep could be induced, for a given load, by raising the temperature and in this case, steady state creep was reduced as shown in Fig. 10. At 1300 °C, failure always occurred during tertiary creep. The results obtained during steady state creep are presented in Fig. 11 from 1100 up to 1300 °C as a function of the applied stress together with creep test results on Nextel 650 single fibres at 1100 °C, published by Wilson.[6]

4.2.2. Fracture morphology

General fibre damage inducing creep was observed, whatever the temperature and load conditions. This consisted of grain de-cohesion and cavity formation which could lead to micro-crack formation depending on creep conditions. Fracture resulted from their coalescence.

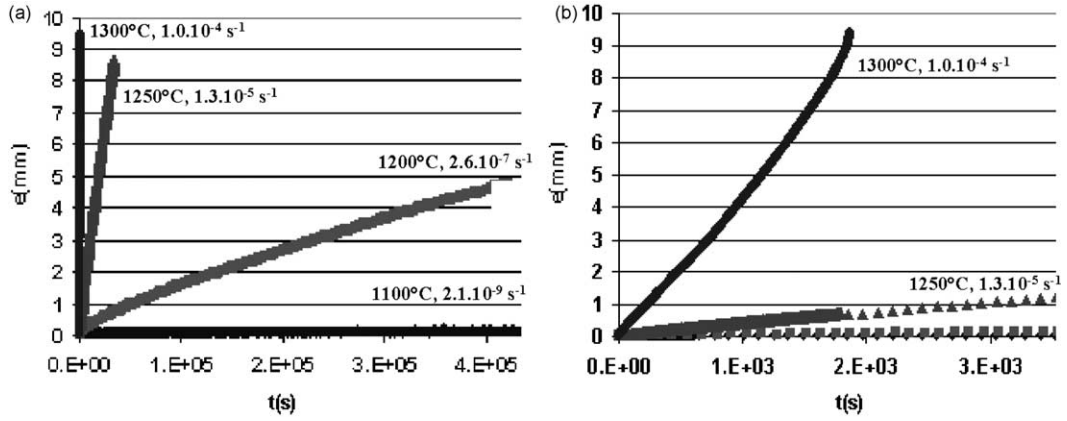

Fig. 10. (a) Displacement–time curves for bundle creep tests from 1100 up to 1300 °C for an applied load of 40 MPa on each bundle fibre (b) Idem. Dilated time scale.

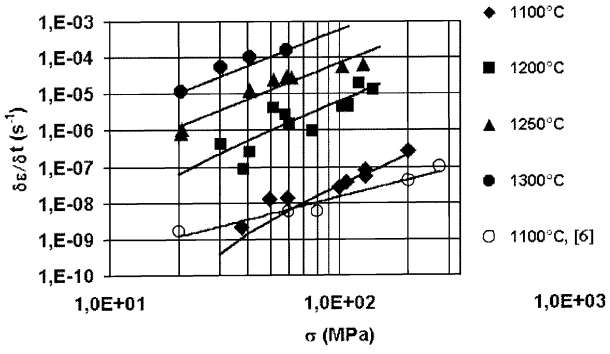

Fig. 11. Creep behaviour from 1100 up to 1300 °C as a function of the applied stress.

At 1100 °C, despite the lengthy tests (from 3 up to 6 days), no grain growth was observed. For high applied stresses (>100 MPa), only fibre surface modification was noticeable with the development of the grain decohesions (see Fig. 12a). However TEM observations showed that intergranular cavities appeared independently of the applied stress and the length of test (see Fig. 13a).

At 1200 °C, damage was comparable to that seen at 1100 °C (formation of cavities) but shorter tests led to failure with usually planar failure surfaces, as shown in Fig. 12b. Small micro-cracks were seen perpendicular to the fibre axis (i.e. load axis) and were observable all along the fibre even close to the point of failure.

At 1250 °C, the damage mode depended on the applied load. For the lowest stress used, 20 MPa, after 34 h, cavities were not numerous (see Fig. 12c). The slower deformation of the fibres could be accommodated by intergranular diffusion which allowed grain growth alignment with the fibre and load axis, parallel to the applied stress, as can be seen in Fig. 13b. EDX analysis at the planar boundaries of elongated alumina grains showed the presence of Si but also Fe, Zr and sometimes Y elements. At the higher stresses used, accommodation of the deformation was more difficult and led to intergranular cavity formation, as at the lower temperatures (see Fig. 13c).

At 1300 °C, even after 5 hours of test for an applied load of 20 MPa, oriented alumina grain growth, as shown in Fig. 13d, was observable as was the coalescence of cavities forming micro-cracks perpendicular to the fibre axis (see Fig. 12d). For higher applied loads, rapid failure always occurred by the coalescence of micro-cracks (see Fig. 12e) and the average grain growth was lower. Some failure surfaces showed abnormal alumina grain growth comparable to those observed after tensile tests at high temperature (see Section 5.1). For bundles, this abnormal grain growth was not the only cause of failure, as damage by coalescence of micro-cracks was more critical for the fibres, as shown in Fig. 14.

When deformation was coupled with alumina grain growth (1250–1300 °C), the distribution of zirconia grains was modified. They coalesced into larger grains (size from 0.1 up to 0.5 μm). As a result, the zirconia grain distribution was less homogeneous and decreased the number of alumina grains surrounded by zirconia. The presence of intragranular zirconia grains inside the alumina grains was confirmed by EDX analysis; their distribution was always homogeneous, with no grouping of the grains close to the centre of the alumina grains or at the grain boundaries.

5. Discussion

The microstructure of the Nextel 650, obtained by a sol-gel process using a rapid pyrolysis step, was seen to consist of alumina grains (average size 100 nm) with both inter- and intra-granular zirconia grains. Heat treatment without load at a temperature close to the pyrolysis temperature, allowed the microstructure to evolve in order to reduce interfacial energies.[7,8] During tensile and creep tests, the rate of microstructural change increased induced by the applied stress.

5.1. Consequences of the impurity presence on the microstructural evolution

At high temperature, defect areas composed of platelets or abnormal alumina grains on the fibre surface were responsible for the decrease of strength observed. These abnormal α-alumina grain growths have previously been reported in the literature for α-alumina based materials in the presence of a liquid phase induced by impurities. In bulk alumina, such growth perpendicular to the *c*-axis, can take place at very low concentrations of co-doping such as of $CaO + SiO_2$ or $Na_2O + SiO_2$.[9] The principal characteristics of these platelets are both their planar faces and their rapid growth. Both their anisotropic growth and their growth kinetics can be explained by the simultaneous presence of different types of impurities.[8,9] Moreover during the process of the abnormal grain formation, even if load plays an important role, Deleglise and al. have shown that the abnormal growth in the mullite-alumina Nextel

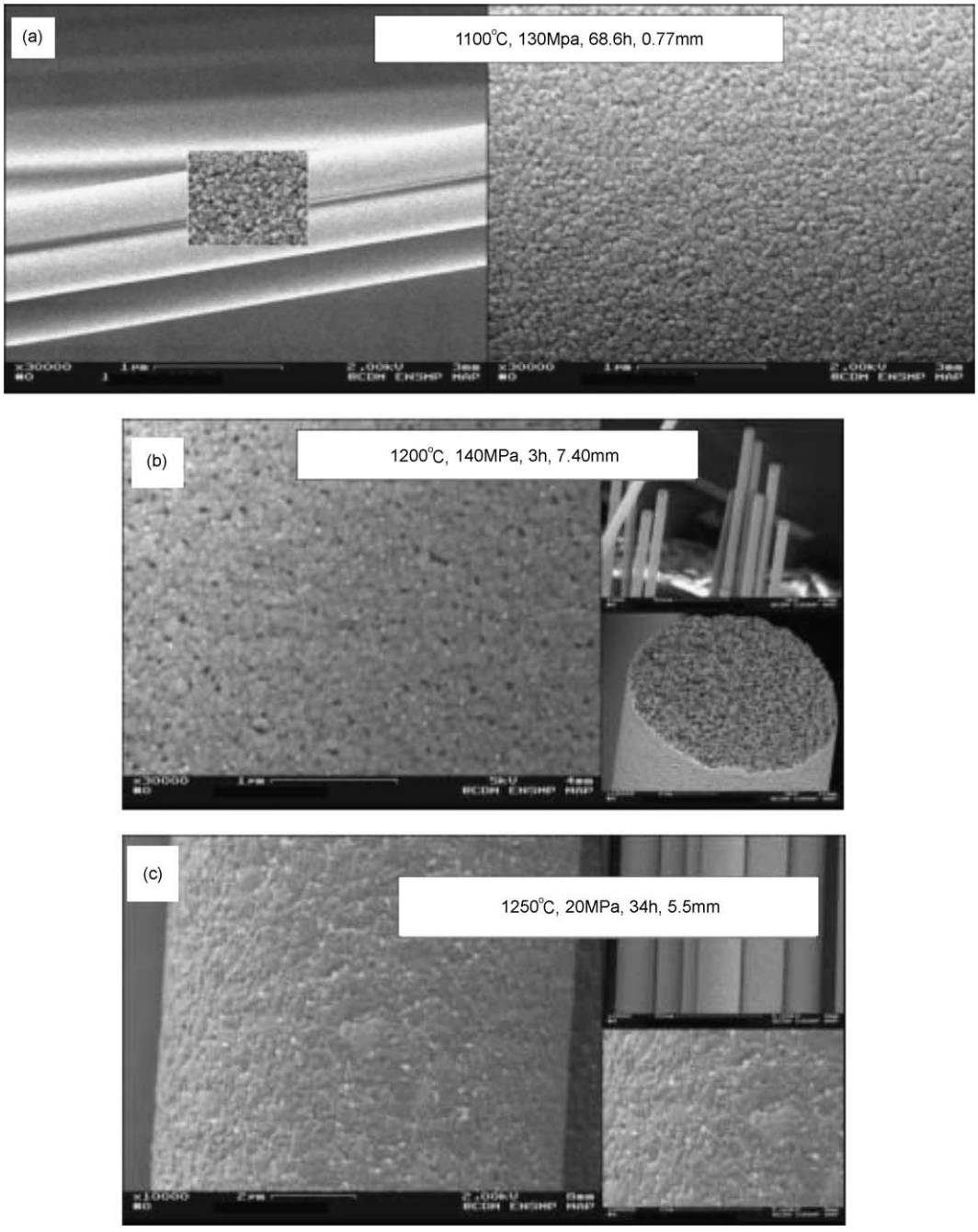

Fig. 12. SEM fibre or failure surface pictures at temperatures from 1100 up to 1300 °C.

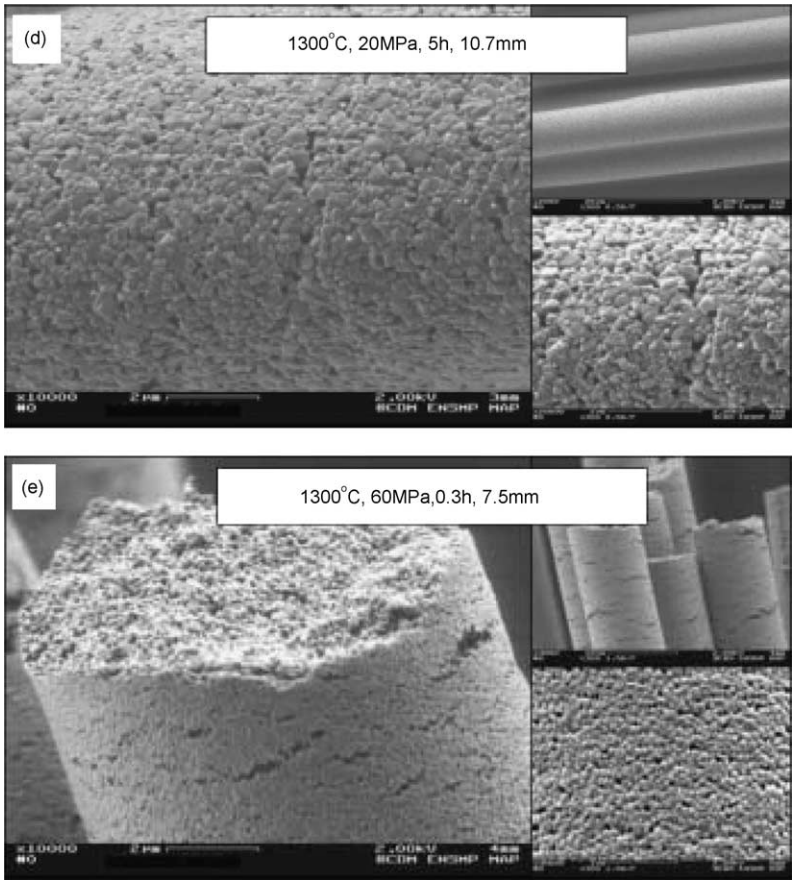

Fig. 12. (*continued*)

720 fibre occurred only above 90% of the failure stress.[10]

For the Nextel 650 fibre, the elements Si and Ca were always present on the EDX spectra when alumina grains showed abnormal growth independently of whether single fibres or bundles were tested. The combination of temperature and load accelerates their growth which is initiated at local chemical heterogeneities. From 720 °C, the ternary phase diagram of ther Al_2O_3–SiO_2–Na_2O system shows the existence of liquid phase. The combination of thin inter-granular liquid films responsible for the faster transport of aluminium ions and the anisotropic interfacial energy and solubilities of Al_2O_3 atomic planes induce the formation of elongated platelike grains, in the presence of CaO or Na_2O, with flat boundaries along the long axis which corresponds to the basal plane as this is the lowest energy plane [9]. These platelike grains were observed on fracture surfaces after tensile tests at high temperature but also on fibre surfaces after heat treatment for 7 days, without load, at 1100 °C, due to concentrations of chemical heterogeneities. The applied load increases dramatically the growth rate but is not necessary for their abnormal growth to occur. This is primarily related to local concentration of impurities (Ca or Na).

5.2. Microstructural evolution during creep

Two different processes of microstructural evolution were noticed during creep : first, overall grain growth parallel to the fibre axis at low applied stresses (with the presence of glassy films at grain boundaries) and second, intergranular cavity formation. In the former case, the intergranular zirconia grains were re-organized and grouped together. Consequently, the zirconia grain distribution was modified and became less homogeneous inside the fibre leading to numerous triple points without any zirconia grains. The fibre was able to accommodate deformation by diffusion leading to an anisotropic microstructure during creep. At high stresses, the diffusion kinetics for deformation accommodation were not sufficient and led to inter-granular cavity formation. The preferential orientation of the alumina grains in the as-received fibres with their basal plane parallel to the fibre axis favoured the growth of platelike grains parallel to the load axis.

The evolution to a microstructure composed of aligned grains oriented parallel to the fibre axis improved the creep properties of the fibre. For sol-gel materials, the choice of a precursor composed of elongated particles able to be aligned inside the fibre during

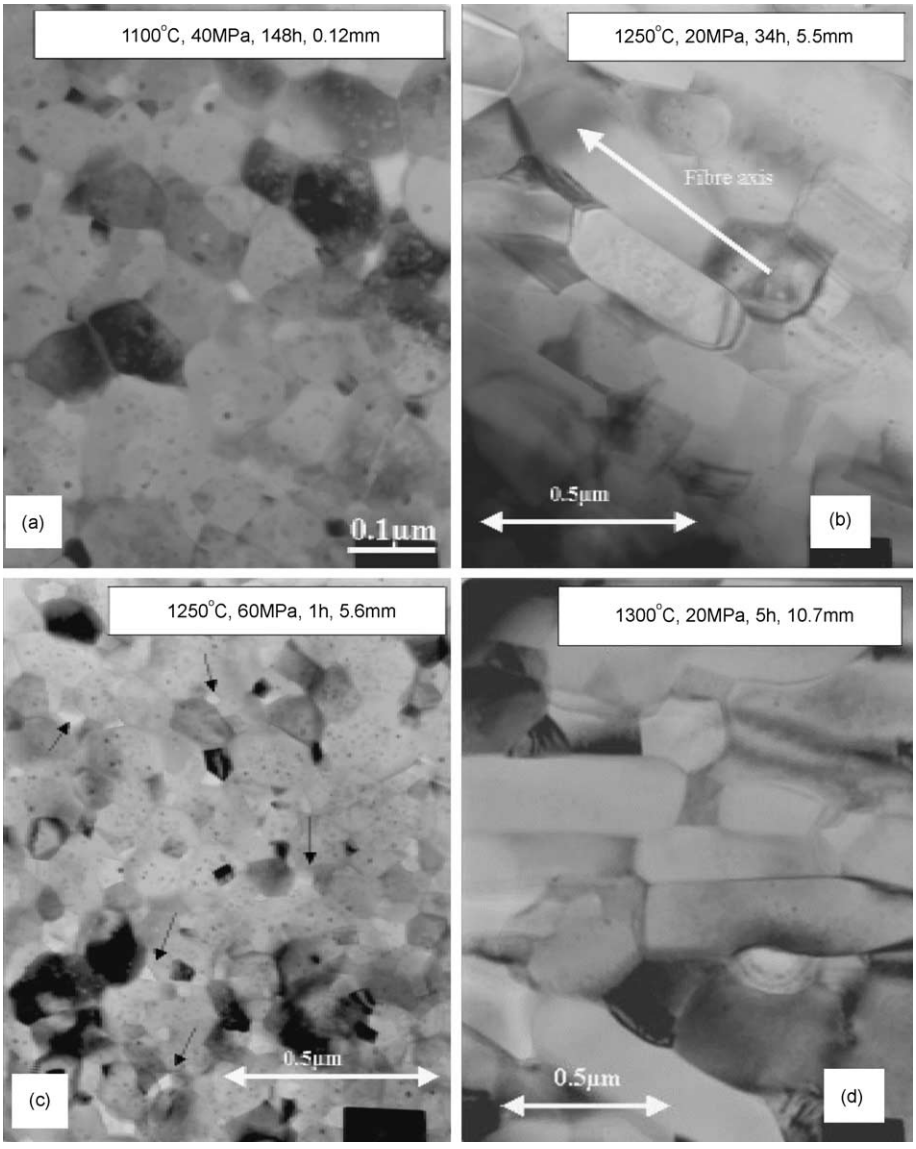

Fig. 13. TEM fibre microstructures after creep tests from 1100 up to 1300 °C.

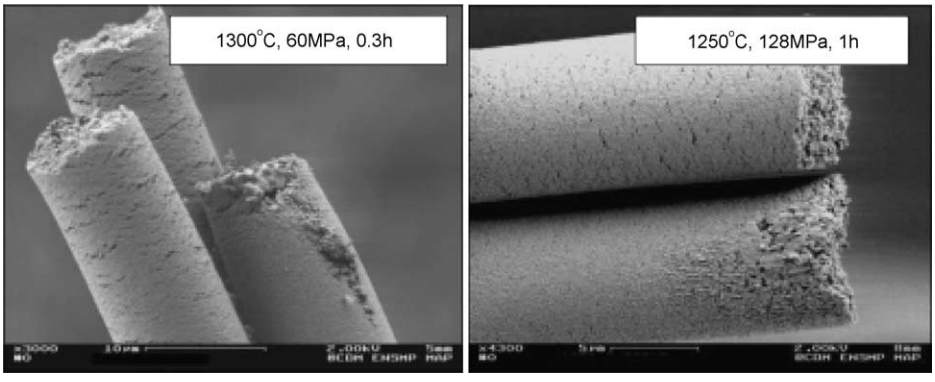

Fig. 14. Abnormal grain growth observed on failure surface after creep on bundles at 1300 °C, 60 MPa and 1250 °C, 128 MPa.

extrusion, can favour the oriented growth of the α-alumina grains[10] but selected dopant additions made during processing, can also explain the fibre microstructure evolution. Alpha-Fe_2O_3 particles added as sintering aids for temperatures lower than 1300 °C, lead to uniform and dense microstructures for α-alumina based materials. For higher temperatures, an anisotropic α-alumina grain growth of platelets due to the presence of Fe^{2+} is reported.[15] Gordon and Ikuma have shown an increase of the diffusion phenomenon at grain boundaries in the presence of iron,[16] which is increased by the oxygen partial pressure. The presence and the quantity of Fe^{2+} have direct consequences on the diffusion of aluminium ions at grain boundaries. Fe^{3+} which is initially present, is reduced to Fe^{2+}. In order to maintain the electric neutrality of the crystal, interstitial aluminium ions and oxygen vacancies are created following Eqs. (1) and (2):

$$O_O^x + 2Fe_{Al}^x = 2Fe'_{Al} + V_O^{\cdot\cdot} + \frac{1}{2}O_{2(g)} \quad (1)$$

$$3O_O^x + 2Al_{Al}^x + 6Fe_{Al}^x = 6Fe'_{Al} + 2Al_i^{\cdot\cdot\cdot} + \frac{3}{2}O_{2(g)} \quad (2)$$

Fe^{2+} segregation at grain boundaries and dissolution in liquid intergranular films occur because of the low solubility of this species in the alumina crystal (from 0.7 up to 1.9% at 1450 °C). Segregation of iron at non basal grain boundaries increases the Al^{3+} diffusivity which leads to rapid grain growth. This phenomenon can also explain the evolution of the Nextel 650 fibre microstructure at low applied stresses, even if a glassy phase, due to the presence of Si, has been observed at some grain boundaries. Co-doping with iron can modify these defects. Wilson et al. have shown that when combined with iron additions, the presence of silicon in quantities sufficiently low to avoid the creation of glassy phases, can inhibit creep without microstructural changes.[3] The increase of the Al^{3+} inter-granular diffusivity can be limited by the presence of Si^{4+} giving a modification of the Eq. (2) equilibrium (i.e. modification of the defect concentration in the alumina lattice). The effect of a co-doping of Si^{4+} and a bivalent ion on Al^{3+} diffusion in solid/solid interfaces has been studied by Gavrilov et al.[19] Intergranular solubility of dopant elements such as Mg^{2+}, can be increased by the presence of silica. A decrease of the Si^{4+} segregation rate can prevent glassy phase formation which changes the grain morphology during growth. In the case of magnesia, if there is more Mg^{2+} than Si^{4+}, abnormal growth is impossible and grain morphology is comparable to that obtained by MgO-doping. As equimolar additions of MgO and TiO_2 increase TiO_2 solubility in alumina by defect compensation reactions [20], Gavrilov et al. have suggested two equations to explain the increase of solubility of doping elements in the case of co-doping [19]:

$$MgO + SiO_2 \xrightarrow{Al_2O_3} Mg_{Al}' + Si_{Al}^{\cdot} + 3O_O^x \quad (3)$$

$$Mg_{Al}' + Si_{Al}^{\cdot} + 3O_O^x \rightarrow \left[Mg_{Al}'\text{-}Si_{Al}^{\cdot}\right]^x + 3O_O^x \quad (4)$$

Eqs. (3) and (4) can be adapted for the case of simultaneous addition of FeO (Fe^{2+}) and SiO_2 (Si^{4+}) and can explain the behaviour observed by Wilson when comparing the Nextel 610 fibre and a pure alumina fibre containing Fe_2O_3. Compared to the isotropic grain growth seen in the PRD-166 fibre, the different alumina grain morphology after heat treatment or creep, in the Nextel 650 fibre, can be partially attributed to the presence of Fe^{2+} ions. However, for the Nextel 650 fibre, even if these species are present at the grain boundaries, zirconia and yttria are also present and other mechanisms are necessary to explain the platelet grain growth observed other than the presence of a glassy phase. Moreover, a necessary but not sufficient condition to produce platelet grain growth of α-alumina grains is the presence of cations (Si^{4+}) with valency superior to the Al^{3+} valency and of another with a lower valency.[17,18] Limiting the presence of SiO_2 and adding zirconia as a second phase gives better creep results than those obtained with the Nextel 610 fibre.[3] In this case, the presence of Zr^{4+} and Y^{3+} at grain boundaries limits the creep but also allows oriented grain growth under particular conditions due to the presence of Fe^{2+}; the disastrous effect on creep of which is counterbalanced by Si^{4+}.

5.3. Mechanisms of creep deformation

At high temperature, the variation of the steady creep rate $\delta\varepsilon/\delta t$ as a function of the applied stress σ and the temperature T can be fitted with the general expression (simulation results represented by continuous lines in Fig. 11).

$$\delta\varepsilon/\delta t = A.\exp(-Q/RT).(\sigma\text{-}\sigma_s)^n$$

with Q the activation energy for creep equal to 850 kJ/mol, n the stress exponent equal to 2.5 and A a constant depending on the material, the grain size and the mechanism controlling the deformation, here determined as 10^5 s^{-1} MPa^{-n}.

For 1100 and 1200 °C, the use of σ_s, a threshold stress representative of a stress limit under which there was no creep, was necessary to fit the curves correctly (equal to 15 and 5 MPa respectively). For Wilson's results at 1100 °C, the threshold value obtained was higher but small compared to the 90MPa value estimated by Lavaste et al. for the PRD-166 fibre of DuPont based on the same system (with 20 wt.% ZrO_2 and larger grain sizes). This illustrates the pinning role played by the zirconia grains.

Whatever the applied stress value, the estimated activation energy was higher than those found in the literature for a pure alumina (410 kJ/mol, 100 MPa)[11] or iron doped (616 kJ/mol)[12] or containing from 0.1 up to 10 wt.% of zirconia (2.5 mol% Y_2O_3, Q 650 and 700 kJ/mol respectively).[11,13] An increase of the activation energy value and the presence of cation elements segregated at grain boundaries inevitably results in an improvement in creep properties. A comparison with the values found for the Nextel 610 fibre (3M's pure alumina fibre, 644 kJ/mol)[14] and the PRD-166 (600 kJ/mol),[14] suggests that the high value obtained (850 kJ/mol) for the Nextel 650 was due to the yttrium segregation at grain boundaries.

A decrease of the creep rate up to 1200 °C, is observed for alumina containing second phase zirconia grains stabilised by yttrium, due to the segregation of Y^{3+} and Zr^{4+} at grain boundaries. If iron is segregated at grain boundaries in alumina,[12] creep rate normally increases but co-doped with other elements its presence can be beneficial for creep.[3] For the Nextel 650, the presence of these elements at grain boundaries was not determined with certainty but an increase of the quantity of iron was evident.

A single model can describe the Nextel 650 fibre creep process leading to the two different evolutions of the microstructure during creep as the principal characteristics were strains to failure of less than 25%, ultimate failure due to crack coalescence and when grain growth occurred, growth parallel to the fibre axis.

A cavitation creep or an interface reaction model are not adequate because the iron at the grain boundaries has to be taken into account and, as for the case of a silica, the iron combined with calcium or sodium can also explain platelet alumina grain growth.[15] A diffusion creep mechanism is the more common process governing creep by accommodating grain boundary sliding by diffusion phenomena.

It is here proposed that the Nextel 650 creep mechanism can be separated into two sequential mechanisms (Fig. 15). The first is an interfacial reaction involving the dissolution and re-precipitation at grain boundaries of aluminium ions, allowing grain growth and secondly grain boundary sliding, each dominating, respectively at low or high applied stresses for the same temperature. In both cases, strain rate is controlled by alumina and oxygen ion diffusion at grain boundaries and highly influenced by the presence of Fe^{2+}, Y^{3+}, Zr^{2+} and Si^{4+}.

At high stresses, material integrity cannot be conserved because of the very high deformation speeds. Pores appear even if diffusion occurs. At low stresses, during grain growth, the Al^{2+} and O^{2-} ion diffusion phenomenon is oriented because of the applied stress. Ions are deposited on grain faces perpendicular to the tensile axis with the help of the presence of a glassy phase which facilitates ion transportation. Grain boundary sliding leads to the re-arrangement and coalescence of zirconia grains during deformation.

5.4. Comparison with other oxide fibres

Fig. 16 shows the creep behaviour from 1100 to 1300 °C of different fibres: FP and Nextel 610 represent pure alumina fibres, PRD-166 zirconia–alumina fibres and Nextel 720 alumina–mullite fibres. There are three different parameters distinguishing these fibres: grain sizes, second phase and inter-granular elemental segregation at Al_2O_3/Al_2O_3 grain boundaries.

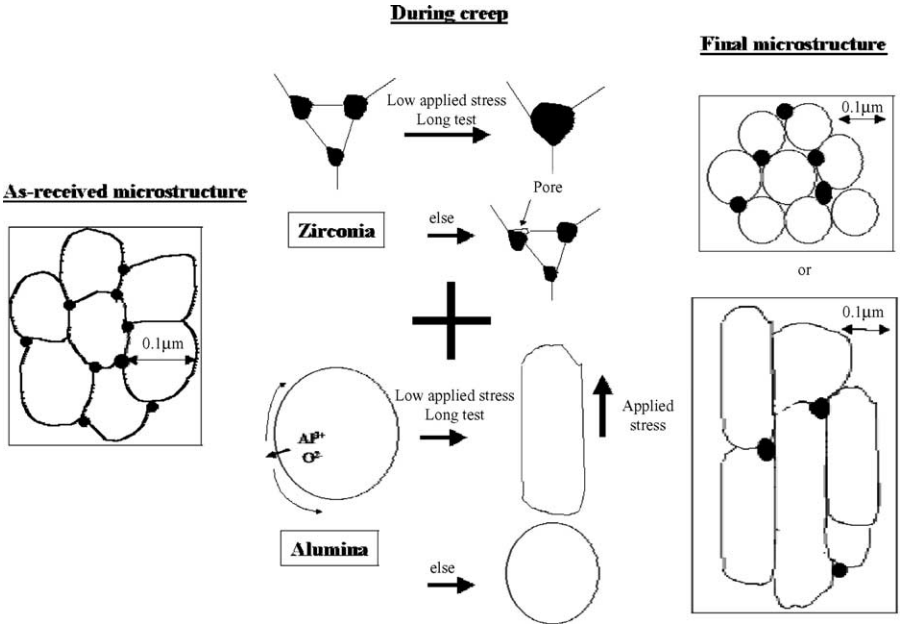

Fig. 15. Diagram showing the creep mechanism of the Nextel 650 fibre.

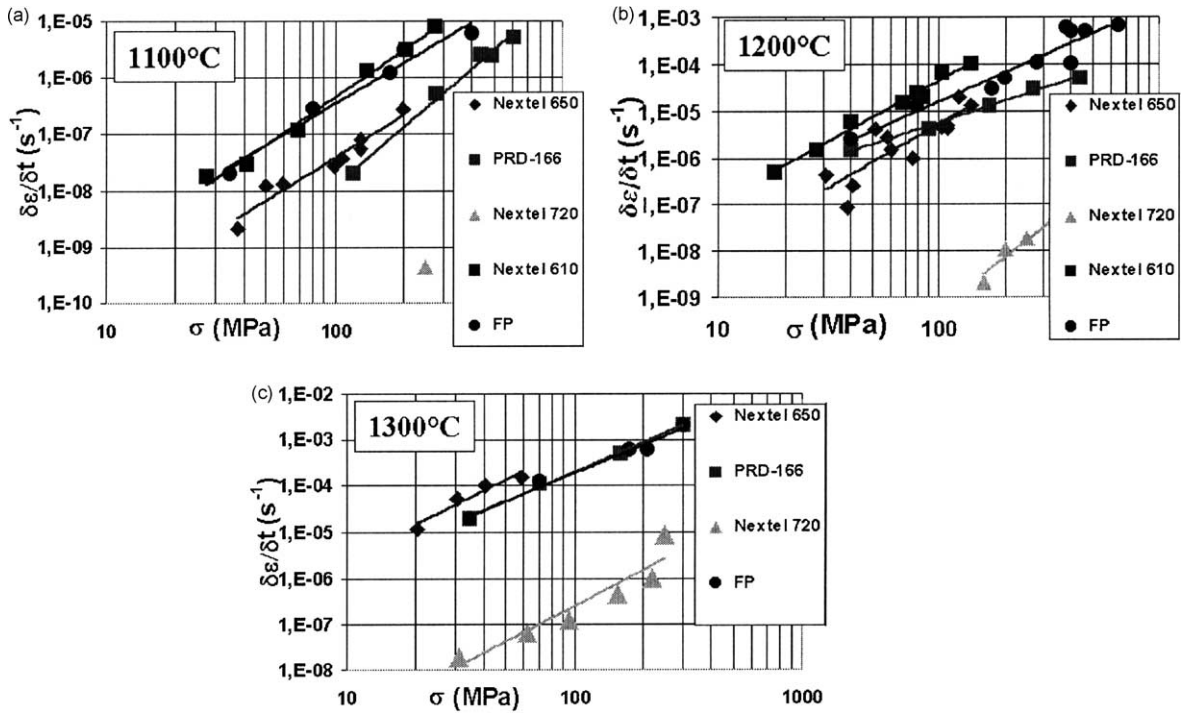

Fig. 16. Comparison with other oxide fibres: FP and Nextel 610 for pure alumina fibres, PRD-166 for zirconia–alumina fibres and Nextel 720 for alumina–mullite fibres.

At 1100 °C, Fig. 16a, the advantages of yttrium stabilised zirconia additions are obvious, taking into account the results obtained for the Nextel 610 (pure alumina fibre) and the Nextel 650 fibres which have identical grain sizes. This structure also overcomes the effects of the smaller alumina grain sizes of these Nextel fibres when comparing the FP and the Nextel 650 fibre results (0.5 and 0.1 μm respectively). Cubic zirconia phase stabilisation obtained by adapting the yttria content are supposed responsible for higher Y^{3+} segregation levels at the Al_2O_3/Al_2O_3 grain boundaries which improves the Nextel 650 fibre creep properties compared to those of the PRD-166 fibre (20% tetragonal zirconia, larger grain sizes) thanks to a co-doping mechanism (Zr^{4+}-Y^{3+}).

Fig. 16b shows a comparison of the creep of Nextel and DuPont fibres at 1200 °C. All the fibres comprised small grains and large boundary surfaces which were available for inter-granular deformation processes. The improvement of creep rates obtained by the addition of zirconia is evident. The creep rates of the Nextel 650 are reduced by one order of magnitude when compared to the Nextel 610 pure alumina fibre at 1100 and 1200 °C.

At 1300 °C, Fig. 16c reveals that the presence of zirconia has no effect on the creep phenomenon (Cf. PRD-166/FP)[1] and the difference between the grain sizes can explain why the PRD-166 fibre shows creep rates of around one order of magnitude lower than those of Nextel 650 fibre.

Although the Nextel 720 (alumina-mullite) fibre shows high sensitivity to its environment at high temperature which renders it chemically unstable, this fibre shows, at 1300 °C, creep rates 5000 times lower than those of the Nextel 650 fibre. These excellent creep properties are due to the presence of a mullite phase but also to the evolution of the microstructure towards a structure finally composed of elongated α-alumina grains. This microstructure is obtained only under particular creep conditions for the Nextel 650 fibre.

6. Conclusion

The combination of sub-micron zirconia and alumina grains leads to the specific mechanical behavior of the Nextel 650 fibre. This study has revealed that up to 1200 °C, the Nextel 650 fibre exibited the properties of flexibility and chemical stability required for use in CMCs.

The aim of 3M was to create a fibre of small diameter (11.2 μm) and grain size of 0.1 μm, able to possess, at room temperature, high tensile strength (2.3 GPa) and capable of conserving a high strength at high temperature, thanks to second phase additions. Creep properties were to be better than those of the Nextel 610 pure alumina fibre and the fibre should present better chemical stability to alkaline environments compared to the Nextel 720 alumina–mullite fibre, without catastrophic grain growth.

The first goal has been attained. Regarding the second, even though the Nextel 650 creep properties are

better than those of the Nextel 610 fibre, they are still inferior to those of the Nextel 720 fibre. Although the Nextel 650 can be described as chemically stable up to 1200 °C it is not totally insensitive to the presence of alkali which explains the abnormal alumina grain growth localized at regions of surface heterogeneities. At higher temperatures, the pinning effect of the zirconia grains is less obvious than in the PRD-166 fibre.

However, because under particular conditions the fibre microstructure can move to an oriented microstructure composed of elongated grains parallel to the load axis, the Nextel 650 can be used with success under high temperature creep conditions. For in-service temperatures lower than 1200 °C, Nextel 650 fibres can be used in composites because its stability during the composite manufacture, even in the presence of small quantities of alkali, is sufficient. Moreover, because its creep properties are better, Nextel 650 fibres can be successfully substituted for Nextel 610 fibres in composites for high temperature applications.

References

1. Lavaste, V., Berger, M. H., Bunsell, A. R. and Besson, J., Microstructure and mechanical characteristics of α-alumina-based fibres. *Journal of Materials Science*, 1995, **30**, 4215–4225.
2. Deleglise, F., Berger, M. H., Jeulin, D. and Bunsell, A. R., Microstructural stability and mechanical properties of Nextel 720 the fibre. *Journal of the European Ceramic Society*, 2001, **21**, 569–580.
3. Wilson, D. M., Lueneburg, D. C. and Lieder, S. L., High temperature properties of Nextel 610 and alumina based nanocomposite fibres. *Ceramic Engineering and Science Proceedings*, 1993, **14**, 609–621.
4. Berger, M. H. and Bunsell, A. R., Thin foil preparation of small diameter ceramic or glass fibres for observation by TEM. *Journal of Materials Science*, 1993, **12**, 825–828.
5. Hagege, R. and Bunsell, A. R., Fibre reinforcements for composite materials. In *Composite Materials Series, 2*, ed. A. R. Bunsell. Elsevier, 1988.
6. Wilson, D. M. and Visser, L. R., High performance oxide fibres for metal and ceramic composites. *Composites A*, 2001, **32**, 1143–1153.
7. Wilson D. M., Private communication.
8. Deleglise, F., Berger, M. H. and Bunsell, A. R., Microstructural evolution under load and high temperature deformation mechanisms of a mullite/alumina. *Journal of the European Ceramic Society*, 2002, **22**, 1501–1512.
9. Song, H. and Cobble, R. L., Origin and growth kinetics of platelike abnormal grains in liquid phase sintered alumina. *Journal of the American Ceramic Society*, 1998, **81**, 2741–2745.
10. Deleglise, F., *Fibres céramiques oxydes biphasées: relation entre comportement mécanique à haute température et microstructure*. Thèse Ecole des Mines de Paris, 5 juillet 2000.
11. Yoshida, H., Ikuhara, Y. and Sakuma, T., A critical factor to determine the high temperature creep resistance in cation-doped polycrystalline Al_2O_3. *Key Engineering Materials*, 2000, **171–174**, 809–816.
12. Hollenberg, G. W. and Gordon, R. S., Effect of oxygen partial pressure on the creep of polycrystalline Al2O3 doped with Cr, Fe or Ti. *Journal of the American Ceramic Society*, 1973, **56**(3), 140–147.
13. Yoshida, H., Okada, K., Ikuhara, Y. and Sakuma, T., Improvement of high temperature creep resistance in fine-grained Al_2O_3 by Zr4+ segregation in grain boundaries. *Philosophical Magazine Letters*, 1997, **1**(76), 9–14.
14. Hammond, *Creep rupture of an oxide/oxide composite fibre*. Thèse de doctorat, University of Virginia, Mai 2001.
15. Tartaj, J. and Messing, G. L., Anisotropic grain growth in α-Fe_2O_3 doped alumina. *Journal of the European Ceramic Society*, 1997, **17**, 719–725.
16. Gordon, R. S. and Ikuma, Y., Creep of doped polycristalline magnesium and aluminium oxides. In *Deformation of Ceramics Materials II*, ed. R. E. Tressler and R. C. Bradt. Plenum Press, 1984, pp. 341–352.
17. Song, H. and Coble, R. L., Origin and growth kinetics of platelike abnormal grains in liquid-phase-sintered alumina. *Journal of the American Ceramic Society*, 1990, **73**(7), 2077–2085.
18. Song, H. and Coble, R. L., Morphology of platelike abnormal grains in liquid phase-sintered alumina. *Journal of the American Ceramic Society*, 1990, **73**(7), 2086–2090.
19. Gavrilov, K. L., Bennison, S. J., Mikeska, K. R. and Levi-Setti, R., Grain boundary chemistry of alumina by high resolution imaging SIMS. *Acta Materialia*, 1999, **47**(15–16), 4031–4039.
20. Roy, S. K. and Coble, R. L., Solubilities of magnesia, titania, and magnesium titanate in aluminum oxide. *Journal of the American Ceramic Society*, 1968, **5**(1), 1–6.